

The effects of processing parameters on mechanical properties of 3D-printed polyhydroxyalkanoates parts

Juan Ivorra-Martinez, Miguel Ángel Peydro, Jaume Gomez-Caturla, Lourdes Sanchez-Nacher, Teodomiro Boronat & Rafael Balart

To cite this article: Juan Ivorra-Martinez, Miguel Ángel Peydro, Jaume Gomez-Caturla, Lourdes Sanchez-Nacher, Teodomiro Boronat & Rafael Balart (2023) The effects of processing parameters on mechanical properties of 3D-printed polyhydroxyalkanoates parts, *Virtual and Physical Prototyping*, 18:1, e2164734, DOI: [10.1080/17452759.2022.2164734](https://doi.org/10.1080/17452759.2022.2164734)

To link to this article: <https://doi.org/10.1080/17452759.2022.2164734>



© 2023 The Author(s). Published by Informa UK Limited, trading as Taylor & Francis Group



Published online: 13 Jan 2023.



Submit your article to this journal [↗](#)



Article views: 173



View related articles [↗](#)



View Crossmark data [↗](#)

The effects of processing parameters on mechanical properties of 3D-printed polyhydroxyalkanoates parts

Juan Ivorra-Martinez , Miguel Ángel Peydro , Jaume Gomez-Caturla , Lourdes Sanchez-Nacher, Teodomiro Boronat  and Rafael Balart 

Institute of Materials Technology (ITM), Universitat Politècnica de València (UPV), Alcoy, Spain

ABSTRACT

The crystallisation process of polyhydroxyalkanoates (PHA) polymers plays a key role on final properties of manufactured parts due to most PHA are highly sensitive to physical aging which leads to embrittlement. The secondary crystallisation associated with the aging process can be partially controlled by the cooling process during manufacturing or, even, by heat treatments such as annealing. A critical parameter in additive manufacturing is the difficulty to achieve good adhesion of the material to the printing bed. The bed temperature plays a key role on PHBH crystallisation, which leads to shrinkage having a negative effect on polymer-to-bed adhesion. In this work, a study of the effect of different processing parameters such as the printing temperature, the bed temperature, the cooling conditions, as well as raster direction on the final properties of PHBH 3D-printed parts is carried out.

ARTICLE HISTORY

Received 9 October 2022
Accepted 29 December 2022

KEYWORDS



Mechanical properties;
optimisation; PHA; PHBH

1. Introduction

The idea of 3D printing was developed by Charles Hull in the 1980s through the development of the first stereo lithography apparatus (SLA) printer (Hull 1998). It was not until 1989 when Scott Crump developed the fused deposition modelling (FDM) technology (Crump 1989; Gardan 2019). Since then, the use of additive manufacturing techniques has become particularly important, and their use is set to lead to the next industrial revolution (Singh and Jonnalagadda 2020). The principle of operation of FDM technology is focused mainly on thermoplastic polymers. Among the different FDM techniques, the Fused Filament Fabrication (FFF) is the most common. In this case, a prefabricated filament is extruded through the nozzle by a roller-based extruder that pushes the filament into the heating zone (Singh et al. 2020). As an alternative to filament printers, some FDM machines replace the roller-based extruder by a single-screw extruder that feeds the nozzle thus allowing direct 3D printing with pellets. By applying heat and shear, pellets are melted progressively along the screw to achieve a homogeneous melt that can feed the nozzle to give 3D-printed parts (Gonzalez-Gutierrez et al. 2018; Liu et al. 2019; Singamneni et al. 2018).

Heating polymers above their characteristic melting temperatures (T_m , for semicrystalline polymers), or

above their glass transition temperature (T_g , for amorphous polymers) allows the polymer to flow through a nozzle. In this way, the fused material is deposited in a controlled way following a selected pattern. The process allows the stacking of layers to finally achieve the desired geometry. By using this technique, it is possible to generate complex shapes without using complex and high-cost equipment (Gonzalez-Gutierrez et al. 2018). Some of the most commonly used materials in FDM are poly(lactic acid) (PLA) and poly(acrylonitrile-butadiene-styrene) (ABS) (Solomon, Sevvell, and Gunasekaran 2020). While ABS is an amorphous petroleum-derived copolymer with good impact resistance, PLA can be obtained from renewable resources and it is easier to print (Rodríguez-Panes, Claver, and Camacho 2018; Bermudez et al. 2021). Among the different thermoplastics currently available on the market, it is worthy to note the increasing use of polyhydroxyalkanoates (PHA) which have been proposed as the bioplastics of the future. PHA include a wide family of polymers that are accumulated in the cells of some microorganisms in a controlled environment of a carbon source such as food industry wastes (Anjum et al. 2016; Kovalcik 2021). As PLA, PHA are biopolymers that can be disintegrated in compost soil which made them an interesting solution for the manufacturing of single use products like

CONTACT Juan Ivorra-Martinez  juaivmar@doctor.upv.es  Institute of Materials Technology (ITM), Universitat Politècnica de València (UPV), Plaza Ferrandiz y Carbonell 1, 03801, Alcoy, Spain

This article has been corrected with minor changes. These changes do not impact the academic content of the article.

© 2023 The Author(s). Published by Informa UK Limited, trading as Taylor & Francis Group

This is an Open Access article distributed under the terms of the Creative Commons Attribution-NonCommercial License (<http://creativecommons.org/licenses/by-nc/4.0/>), which permits unrestricted non-commercial use, distribution, and reproduction in any medium, provided the original work is properly cited.

packaging. Also they are biocompatible and resorbable which give a great potential for the manufacture of medical devices so they can be introduced inside the human body and eliminated due to they are bioabsorbable or resorbable (Diederichs et al. 2019; Kovalcik 2021). Additionally, the introduction of additive manufacturing techniques in medicine is gaining special interest due to the possibility of manufacturing medical customised devices to the special needs of each patient (Kumar, Kumar, and Chohan 2021).

Currently, it is possible to find a wide number of materials based on PLA. Even more, some recent developments offer a full PHA filament for 3D-printing (allPHA by colorFabb). Nevertheless, PHA was usually blended (up to 20–25%) with PLA to enhance good processability to tailor the desired properties (Menčík et al. 2018; Relinque et al. 2019; Kovalcik 2021). Kovalcik et al. showed that poly(3-hydroxybutyrate) (PHB) or poly(3-hydroxybutyrate-co-3-hydroxyvalerate) (PHBV) can undergo degradation during hot-melt processing, since their working temperature is very close to the degradation temperature making it difficult to obtain the corresponding filament. However, they concluded that poly(3-hydroxybutyrate-co-3-hydroxyhexanoate) (PHBH) has less degradation during processing and, therefore, PHBH is a good candidate to obtain filaments for 3D-printing (Kovalcik et al. 2020). In spite of the fact that PHBH is less sensitive to thermal degradation during processing compared to other PHA, it stills suffers more degradation than PLA. Consequently, the use of a pellet printer avoids one thermal cycle required to obtain filaments from pellets. Another advantage of using extrusion-based 3D printer is the possibility of working with continuous fibre as a reinforcement, which widens the potential of these technologies in engineering applications, since long fibre polymer reinforced parts, can be obtained by additive manufacturing (Liu et al. 2020; Liu, Xiong, and Zhou 2021; Pappas et al. 2021). Another way that has been investigated to obtain PHA parts by additive manufacturing is the use of selective laser sintering techniques which are very helpful to obtain accurate geometries (Pereira et al. 2012).

One of the main problems in 3D-printing is the possibility of warping due to the shrinkage suffered by the material during cooling. To avoid this, a heated bed can help to avoid undesired deformations due to detachment of the first layer. Additionally, an enclosed 3D-printer allows a more homogeneous cooling, which is key for some materials such as ABS. Other parameters like the surface on which the material is deposited, the use of adhesives, or adhesion enhancement methods such as raft, skirt or brim can help to improve adhesion (Menčík et al. 2018; Singh 2018; Morales et al. 2021). In addition to the cooling conditions, shrinkage also occurs in

semicrystalline polymers during crystallisation, with the subsequent negative effect on debonding or warping defects (Spoerk, Holzer, and Gonzalez-Gutierrez 2020).

Depending on the conditions under the crystallisation of PHA takes place, differences in the degree of crystallinity of the material can be obtained. Therefore, the properties of PHA are highly influenced by the cooling conditions (Kabe et al. 2012, 2015). Furthermore, PHBH is a medium-chain length PHA (mcl-PHA), which results in a more flexible behaviour compared to PHB. On the other hand, PHA suffers physical aging at room temperature due to secondary crystallisation which leads to embrittlement (Laycock et al. 2014; Ivorra-Martinez et al. 2020b). Considering this, the thermal treatments after the processing play an important role. Annealing is a very usual applied thermal treatment on semicrystalline polymers subjected to rapid cooling. Annealing is a very useful tool to tailor the final properties of the material due to the different degree of crystallinity obtained, depending on time and temperature (Cherpinski et al. 2017; Yeo et al. 2018).

This research aims to assess the effects of the main processing parameters of a 3D-printing process using PHBH pellets instead of filament to prevent polymer from degradation. More specifically, the effect of the nozzle temperature in the 175–185°C range, the bed temperature in the 60–80°C range and the layer fan cooling activation, on mechanical properties and 3D-printability of PHBH is studied. In addition, the raster angle (transversal and longitudinal) was also evaluated. The study of a PHA in additive manufacturing is interesting for the development of medical devices. Nowadays the development of medical devices that can be resorbable and adapted to the special needs of the patient is gaining special attention. Until now, the number of studies in which a PHA is employed without blending with other polymers is very limited and the effect of the working parameters in additive manufacturing has not been assessed.

2. Materials and methods

2.1 Materials

Poly(3-hydroxybutyrate-co-3-hydroxyhexanoate) (PHBH) grade PH110 from Ercros S.A. (Barcelona, Spain) with a melt flow index (MFI) of 1 g/10 min (ISO 1133-2 at 160°C and 2.16 kg) and a melting temperature of 124°C was used in pellet form. To avoid hydrolysis, PHBH pellets were dried 6 h at 80°C to remove residual moisture.

2.2 3D-printing with PHBH pellets

The tensile test samples were manufactured in a 3D printer Tumaker equipped with a single-screw extruder

to work directly with pellets. This is a side-wall enclosed unit with external dimensions of $450 \times 410 \times 410 \text{ mm}^3$ and a printing volume of $270 \times 190 \times 200 \text{ mm}^3$. The printing process was carried out at a controlled room temperature range between 23 and 25°C. 3DLAC adhesive spray (San Cristóbal de Entreviñas, Spain) was used as an adhesive to ensure correct adhesion of the polymer to the glass bed. The gcode generation was made using Simplify3D 4.1 (Cincinnati, United States) following the conditions provided in Table 1.

The temperatures employed for the manufacture of the samples were chosen according to the observed working range established by an iterative process in which, different temperatures were tested until a good first layer adhesion was obtained in a range from 60°C to 80°C. The proper rotation of the screw was obtained in the 170°C–185°C range. A deeper explanation of the process followed to obtain the working parameters has been done in 'Section 3.4 Printability of PHBH' and considering the results obtained in 'Section 3.3 Thermal characterisation of PHBH'. Regarding the cooling process of the 3D-printed samples, a 5015-fan working at 3500 rpm was assembled next to the hot end (100%-layer fan activation) that produced an air flow directly to 3D-printed sample to increase the cooling rate of the melted deposited polymer.

The flow calibration was performed iteratively. To obtain the extruder steps per millimetre, different tests were carried out initially by using different values. A single wall cube was 3D-printed, and the wall thickness was measured with a micrometer. The steps were calibrated, when a line width of 0.8 mm was reached. A Tesa Technology (Renens, Switzerland) micrometer with a measuring range of 0–25 mm and a precision of 0.01 mm was used for the measurement.

The designation of the samples was made according to the following criteria: Heat zone 1/Bed temperature. The samples with a longitudinal pattern (raster direction aligned with the applied axial loading direction in tensile test) were designated with L, and those with a transverse pattern (raster direction perpendicular to the applied

axial loading direction in tensile test) were designated with T. Additionally, different combinations were analysed with regard to the fan: one consisting on switching the fan on for 100% layers from the second printed layer (F), and another one consisting on switched off fan (NF). Table 2 summarises the main varying parameters for 3D-printing with PHBH.

Due to the influence of temperature on the recrystallisation process, in order to consider the same conditions in all cases, the specimens were processed individually. After ending the 3D-printing process, specimens were left inside the printer until the bed temperature reached room temperature.

2.3 Mechanical properties

Tensile tests samples were 3D-printed and tested according to ISO 527 after a 14-day aging period at room temperature, since these properties are more representative for the long-term behaviour of PHA as reported in literature (Xu et al. 2018). For this purpose, an ELIB 30 universal testing machine from Ibertest (Madrid, Spain) equipped with a 5 kN load cell was used. Each measurement was performed 5 times to obtain an average of the main tensile parameters and the corresponding standard deviation. ANOVA statistical analysis was carried out using Statgraphics 18 (The Plains, USA).

2.4 Infrared spectroscopy characterisation

Chemical structure analysis was performed by ATR-FTIR (attenuated total reflection-Fourier transform infrared). The analyses were carried out with a Vector 22 from Bruker S.A. (Madrid, Spain) to which the ATR accessory was supplied by PIKE Technologies (Madison, USA). Ten measurements with a precision of 4 cm^{-1} and a range of $4000\text{--}700 \text{ cm}^{-1}$ were performed.

2.5 Fracture morphology

Images of the tensile test specimens fractured surface morphology were taken by means of ZEISS ULTRA 55 microscope from Oxford Instruments (Abingdon, UK) with an acceleration voltage of 2 kV. Prior to collecting the images, a sputtering process was performed with gold-palladium alloy in a SC7620 sputter coater from Quorum Technologies Ltd. (East Sussex, UK).

Table 1. Printing parameters used for gcode generation of PHBH 3D-printed materials.

	Value	Unit
Layer height	0.4	mm
Initial layer speed	8	mm/s
Nominal speed	12	mm/s
Layer fan	100 (layer 2) or 0	%
Brim	4 (layer 1)	mm
Nozzle	0.8	mm
Line width	0.8	mm
Wall line count	0	–
Infill	100	%
Raster direction	0 or 90	°

Table 2. Printing conditions used for 3D-printing PHBH-based materials.

Nozzle temperature or hotend (°C)	Bed temperature or heat bed (°C)	Stepper motor (steps/ mm)
175, 180 or 185	60,70 or 80	300

2.6 Thermal properties

Differential scanning calorimetry (DSC) was used to assess the thermal properties of PHBH and, consequently, to establish the working temperatures. The main thermal parameters, namely the glass transition temperature (T_g), the melt peak temperature (T_m), the melting enthalpy (ΔH_m), and the degree of crystallinity χ_c (%) were obtained from the corresponding DSC runs. The degree of crystallinity was calculated with equation 1 where ΔH_m^0 is the melt enthalpy of a theoretically fully crystalline sample of PHBH, which was considered as 146 J/g as reported in literature (Mahmood et al. 2020), and ΔH_m is the obtained melt enthalpy for PHBH.

$$\chi_c(\%) = \frac{\Delta H_m}{\Delta H_m^0} \cdot 100 \quad (1)$$

DSC runs were performed in a DSC Mettler-Toledo Inc. (Schwerzenbach, Switzerland) under a nitrogen atmosphere (66 mL/min) using a sample weight between 5 and 7.5 mg. The dynamic DSC run was performed from -50°C to 200°C at $10^\circ\text{C min}^{-1}$ to measure the thermal properties of the samples after the aging.

Thermogravimetric analysis (TGA) was carried out in a Mettler-Toledo TGA/SDTA 851 (Schwerzenbach, Switzerland) thermobalance. An average weight of 5–7 mg sample placed into an alumina pan with a total volume of 70 μL , was employed for the test. The dynamic temperature sweep was scheduled from 30°C to 700°C at a constant heating rate of $20^\circ\text{C min}^{-1}$ in nitrogen atmosphere.

3. Results and discussions

3.1 Mechanical properties of the PHBH 3D-printed parts

The mechanical properties of the 3D-printed specimens for tensile tests with the different processing parameters cooled with the layer fan are gathered in Table 3 (transversal raster) and Table 4 (longitudinal raster), while the tensile properties of 3D-printed

Table 3. Summary of the mechanical properties of the samples printed with transversal (T) raster angle and with the layer fan working.

T-F	Tensile strength (MPa)	Elongation at break (%)	Tensile modulus (MPa)
175-60	14.5 ± 0.6	13.6 ± 0.5	760 ± 38
180-60	15.1 ± 0.5	14.4 ± 0.4	817 ± 16
185-60	12.6 ± 0.5	13.3 ± 0.4	765 ± 15
175-70	14.0 ± 0.6	14.0 ± 0.4	699 ± 28
180-70	14.8 ± 0.6	14.5 ± 0.6	770 ± 39
185-70	13.0 ± 0.5	13.3 ± 0.5	682 ± 27
175-80	14.2 ± 0.4	14.4 ± 0.6	649 ± 26
180-80	14.4 ± 0.4	14.5 ± 0.4	707 ± 28
185-80	13.6 ± 0.4	13.6 ± 0.4	645 ± 19

Table 4. Summary of the mechanical properties of the samples printed with longitudinal (L) raster angle and with the layer fan working.

L-F	Tensile strength (MPa)	Elongation at break (%)	Tensile modulus (MPa)
175-60	17.8 ± 0.5	17.0 ± 0.7	846 ± 17
180-60	18.0 ± 0.5	17.3 ± 0.5	847 ± 25
185-60	16.5 ± 0.7	16.1 ± 0.6	795 ± 16
175-70	18.2 ± 0.5	17.1 ± 0.5	801 ± 24
180-70	18.6 ± 0.7	17.2 ± 0.7	804 ± 16
185-70	17.3 ± 0.5	16.1 ± 0.6	757 ± 38
175-80	15.8 ± 0.6	16.5 ± 0.7	746 ± 33
180-80	16.2 ± 0.5	16.4 ± 0.5	758 ± 35
185-80	15.1 ± 0.6	14.9 ± 0.6	737 ± 37

specimens cooled down without the fan are described in Tables 5 and 6 shows the results obtained for those samples cooled without the layer fan. Due to the large amount of data obtained, an ANOVA statistical study was used to determine the differences that arise depending on the selected parameters presented in Figures 1 and 2, respectively.

The ANOVA analysis of the obtained results shows that some parameters have a marked influence (bars above the red line) on the different tensile properties of the 3D-printed samples. Regarding the tensile strength, the raster has a highly remarkable influence. In this case, the best results were obtained in those parameters in which the raster was aligned (L) with the axial load applied during the tensile test. The tensile strength showed lower values for specimens obtained using a transverse pattern (T), since the strength was transferred between adjacent beads. These results agree with those reported by Rajpurohit et al. (2018). They concluded that the fracture in a 3D-printed specimen is related to the separation of the interface of the beams when the other patterns is perpendicular to that of the applied load. This phenomenon is common when characterising samples obtained by 3D-printing, resulting in anisotropy and therefore, the mechanical properties are highly dependent on the selected orientation (Dudescu and Racz 2017; Dizon et al. 2018; Ayatollahi et al. 2020; Dave et al. 2021).

Table 5. Summary of the mechanical properties of the samples printed with transversal (T) raster angle and without the layer fan.

T-NF	Tensile strength (MPa)	Elongation at break (%)	Tensile modulus (MPa)
175-60	15.1 ± 0.3	14.6 ± 0.4	645 ± 19
180-60	15.1 ± 0.6	15.2 ± 0.6	640 ± 13
185-60	14.3 ± 0.3	14.9 ± 0.3	614 ± 12
175-70	14.7 ± 0.7	14.5 ± 0.4	618 ± 25
180-70	14.8 ± 0.4	14.8 ± 0.3	605 ± 12
185-70	14.0 ± 0.3	14.1 ± 0.4	577 ± 29
175-80	*	*	*
180-80	*	*	*
185-80	*	*	*

*Note: Could not be 3D-printed due to excessive warping and detachment.

Table 6. Summary of the mechanical properties of the samples printed with longitudinal (L) raster and without the layer fan.

L-NF	Tensile strength (MPa)	Elongation at break (%)	Tensile modulus (MPa)
175-60	16.2 ± 0.5	15.8 ± 0.5	666 ± 33
180-60	16.3 ± 0.3	16.1 ± 0.5	669 ± 13
185-60	16.0 ± 0.3	15.3 ± 0.8	649 ± 19
175-70	15.4 ± 0.5	15.1 ± 0.8	622 ± 12
180-70	15.3 ± 0.6	15.5 ± 0.5	627 ± 31
185-70	14.5 ± 0.6	14.6 ± 0.7	611 ± 12
175-80	*	*	*
180-80	*	*	*
185-80	*	*	*

*Note: Could not be 3D-printed due to excessive warping and detachment.

Another parameter that had a significant influence on the tensile strength according to the results shown by the ANOVA analysis was the hot-end temperature. This parameter did not show a linear trend; the best results were obtained for the intermediate temperature value considered (180°C). Between 175°C and 180°C an increase in strength was observed, which is probably

related to the improved adhesion between the beads and the 3D-printed samples. As proposed in the work of Alafaghani et al. with PLA, an improvement of tensile strength was observed between 175°C and 190°C. A further temperature increase up to 205°C, did not lead to a significant increase in tensile strength (Alafaghani et al. 2017). However, PHA polymers are particularly sensitive to thermal degradation even at temperatures slightly above the melting temperature (very narrow processing window) (Bordes et al. 2008). For this reason, a decreasing trend for tensile strength can be observed for PHBH 3D-printed samples above 180°C, with 15.1 MPa for 180-60T samples and 12.6 MPa for the 185-60T samples, which means a reduction of 16.5%. The thermogravimetric (TGA) properties in the thermal characterisation show that the onset degradation starts at 277°C, while the maximum degradation rate takes place at a temperature of 309°C. Therefore, no severe degradation is expected by using the temperatures

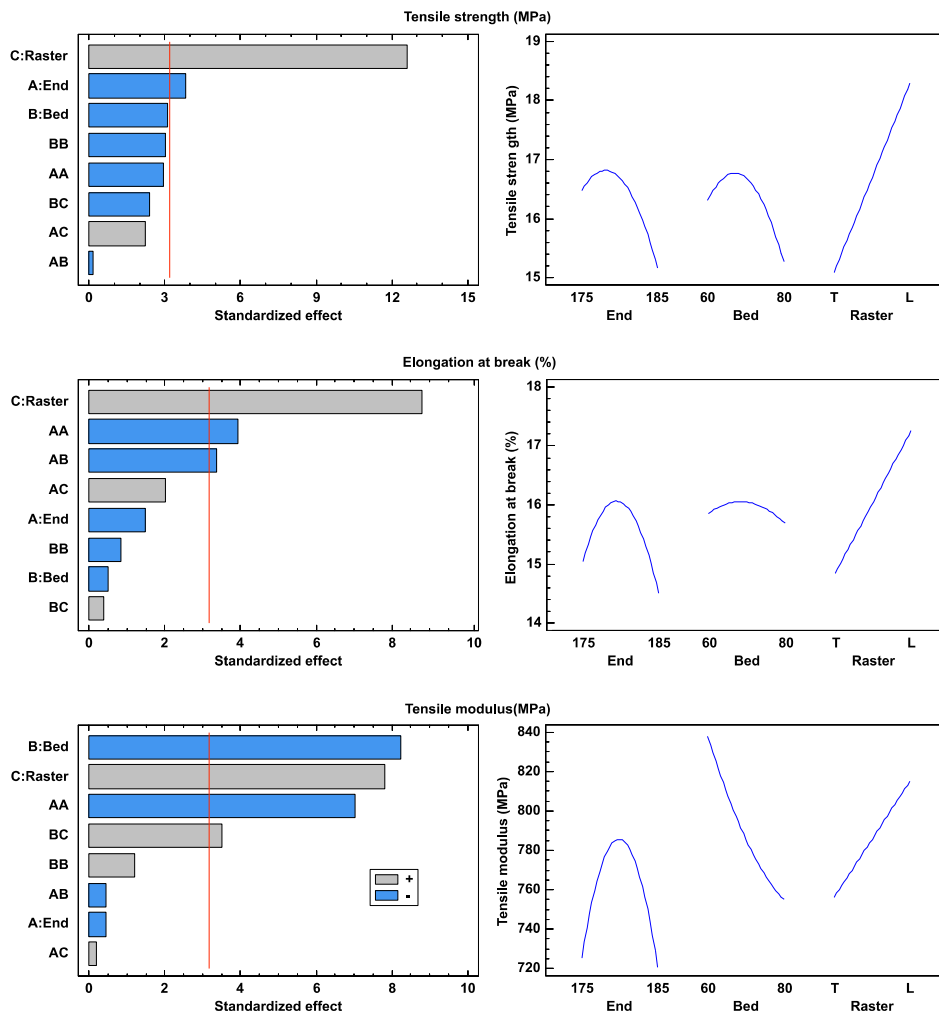


Figure 1. Summary of the ANOVA analysis for PHPH 3D-printed samples by using the layer fan during the cooling process. This shows the Pareto diagram standardised effect (left row) and the main effects diagram (right row) for tensile strength, elongation at break and tensile modulus.

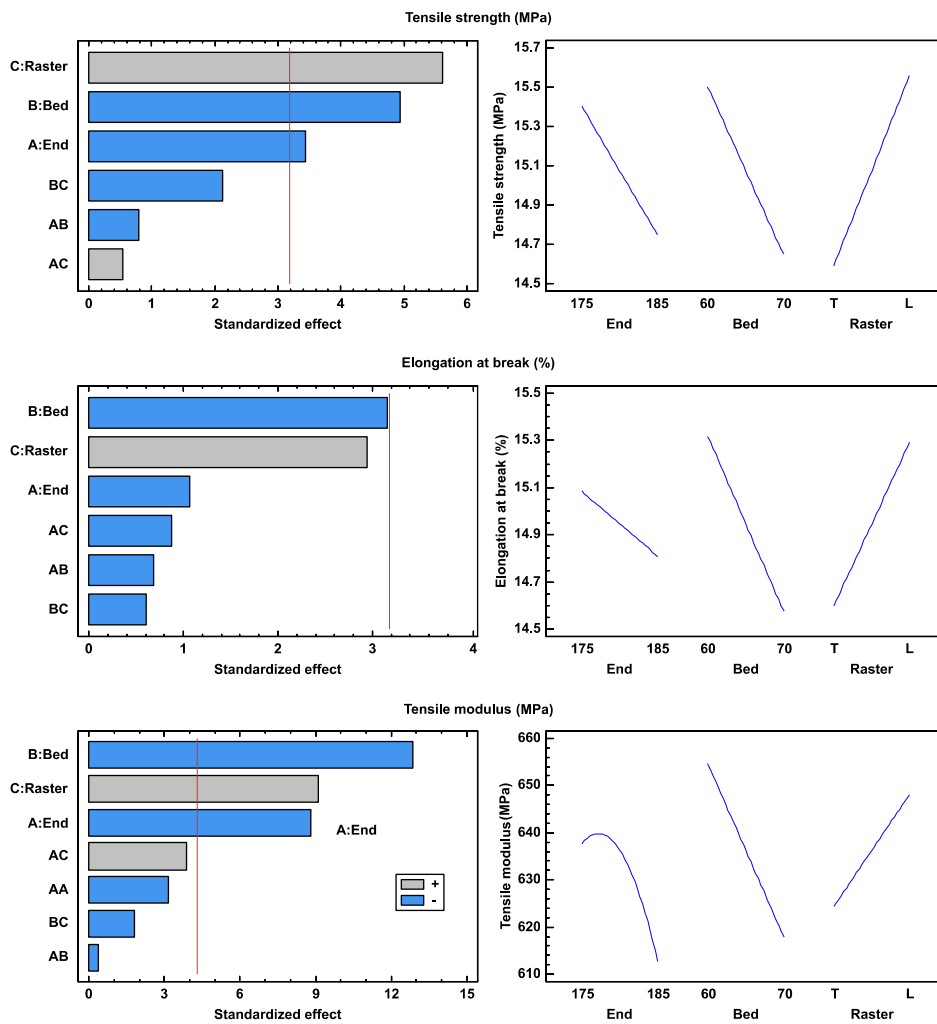


Figure 2. Summary of the ANOVA analysis for PHPH 3D-printed samples by switching off the layer fan during the cooling process. This shows the Pareto diagram standardised effect (left row) and the main effects diagram (right row) for tensile strength, elongation at break and tensile modulus.

employed in the extruder, which are above the melting temperature obtained by DSC and below the onset degradation temperature obtained by TGA. Shojaeirani et al. studied the effect of five extrusion cycles for two biopolymers, namely PLA and PHBV working with a maximum temperature of 166°C for PLA and 177°C for PHBV. Under these conditions, the polymers employed were working at temperatures below their corresponding onset degradation observed by TGA, with a mass loss starting at 287°C for PLA and 251°C for PHBV. As a result of the extrusion cycles performed, the molecular weight of PLA changed from 203,500 g/mol to 44,149 g/mol and for PHBV from 298,500 to 52,262 g/mol confirming that even below the mass loss temperature polymers suffer from thermal degradation, mainly, chain scission (Shojaeirani et al. 2019).

As for the elongation at break, the main parameter with a clear effect on it is the raster angle used. When the raster angle is aligned with the applied load, the

best results are obtained and as expected, the use of a perpendicular raster direction during the 3D-printing, clearly leads to the decreased elongation at break values. While the maximum elongation at break for 3D-printed samples with a longitudinal pattern was 17.3%, by using a transversal pattern the maximum elongation at break was reduced to 14.4%. Such results are in agreement with those reported by Algarni et al. (2021), and Zhang et al. (2019). As proposed above, the samples with a perpendicular pattern are limited by the deposition lines adhesion, as a result, the ability for plastic deformation is somewhat restricted. With regard to the hot end temperature, the best results were obtained at 180°C; above this temperature, the effects of thermal degradation of PHBV are reflected in a decrease in elongation at break due to the narrow processing window of PHA. Samples printed with a longitudinal pattern and same heated bed temperature achieved differences up to 9% by changing the hot end

temperature from 180°C to 185°C. The heated bed had a negligible effect, as the line obtained was practically flat showing no differences between the temperatures considered in this study.

Regarding the tensile modulus of PHBH 3D-printed specimens with different processing parameters, the highest modulus was achieved for a heated bed temperature of 60°C (lowest temperature considered in this study), so the fastest cooling of the sample was achieved. Despite the 3D – printer used in this work has enclosed side walls, there is not any enclosure for the top. In any case, by using a heated bed, the environment surrounding the sample was at a higher temperature than the room temperature and depends on the temperature of the heated bed. This warm environment was equivalent to a post-annealing treatment since specimens were subjected to moderate-to-high temperatures during the printing time, thus enhancing crystallisation. As it has been reported in literature, the mechanical properties of many PHA are highly dependent on the post-processing heat treatments, usually annealing (Kurusu et al. 2014, 2015; Chen et al. 2021). Kurusu et al. (2015) used a post-processing annealing for PHB, and as a result stiffness was increased. Additives can also exert an important effect on the annealing process by accelerating it or slowing down it, depending on the additive, amount, and chemical structure.

For the raster angle, as mentioned above, when the applied load direction is aligned with the pattern, then the highest values were obtained in all the measured parameters (for samples manufactured at the same temperatures). This trend is in accordance with that obtained by Zhang et al. (2019). In this work, different printing parameters were analysed to assess their effect on the final properties of PLA. Among the parameters analysed, the different raster angles were considered. A linear trend could be observed for the tensile modulus against the raster angle with the highest values close to the applied load direction (L), and a decreasing trend when the beams were oriented in perpendicular direction (T). While the highest tensile modulus for samples with a longitudinal pattern was 847 MPa, 3D-printed samples with a transversal pattern reached a slightly lower tensile modulus of 817 MPa, so differences around 3.5% were obtained for the highest values.

After collecting the mechanical properties of 3D-printed specimens obtained with the layer fan switched off, an ANOVA test was carried out to identify the most relevant parameters having a direct influence on final performance. The main mechanical properties are included in Tables 5 and 6, while the ANOVA analysis results can be found in Figure 2. A priori, some

differences can clearly be detected. In this case, the heated bed temperatures considered were only 60°C and 70°C. When the layer fan was switched off the 3D-printing process with PHBH using a heated bed at a temperature of 80°C, clear evidence of warping was observed resulting in defective specimens, and therefore, they could not be tested. This phenomenon is related with the PHBH crystallisation; the slowest cooling conditions allowed the polymer chains to rearrange more easily leading to an increase in crystallinity which, in turn, resulted in higher shrinkage. This shrinkage was responsible for warping and promoted specimen detachment from the heated bed (Spoerk, Holzer, and Gonzalez-Gutierrez 2020).

As for the tensile stress measured for the 3D-printed specimens with the layer fan activated, the most important parameter with the layer fan switched off was the raster angle. This result corroborates the high importance of the direction considered when analysing the results of the mechanical properties of 3D-printed parts, that corroborating the anisotropy, while tensile strength in 175-60T samples was 15.1 MPa, the corresponding 3D-printed samples with a longitudinal pattern offered a slightly higher tensile strength of 16.2 MPa (which represents a percentage variation of 6.7%). Under these conditions, with no layer fan, the effect of the heated bed temperature had a significant influence. The tensile stress was reduced when the heated bed temperature increased, for example, 3D-printed samples with coded as 185-60 L achieved a maximum tensile strength of 16.0 MPa, whilst the 3D-printed samples with the heated bed at 70°C reached a tensile strength of 14.5 MPa which represents a percentage difference of 9%. This is related to the internal structure of PHBH since most PHA, under slow cooling conditions, promote the formation of spherulites that enhance microcrack formation and growing, as proposed by El-Hadi et al. (2002). The presence of these microcracks in the internal structure are responsible for a decrease in material's cohesion, with the subsequent decrease in tensile strength. Safari et al. (Safari and van de Ven 2015), analysed the effect of cooling temperature on the internal structure of PHB films and the effect on final properties. They observed a clear decrease in tensile strength as the cooling rate increased.

Additionally, the temperature used in the hot end also had a negative effect on the tensile strength. In the previous case, the intermediate temperature value (180°C) showed a slight improvement in tensile strength, but regarding specimens with no layer fan, a decreasing tendency of tensile strength was observed with increased hot end temperature. In this case, the reduction achieved was around 5.4% for 3D-printed

samples a heated bed at 70°C and a using longitudinal (L) pattern. This is due to the fact that the improvement in the adhesion between the beads could improve with the increase in hotend temperature (as shown before). This effect was not such an important effect to counteract the thermal degradation.

With regard to elongation at break, the statistical analysis showed that there was no parameter having a clear and relevant influence on it. However, as for samples obtained with layer fan, the heated bed temperature and the raster angle have certain effect over elongation at break. Again, the presence of microcracks in the internal structure results in premature failure and, therefore, in a lower elongation at break. As expected, the use of a longitudinal raster pattern (L) provides higher elongation at break values up to 16.1%, while specimens obtained with transversal pattern (T) led to slightly lower elongation at break values of 15.2%, thus indicating a percentage change of 5.5%. The longitudinal raster pattern provides higher material's cohesion than the transversal raster pattern.

The elastic modulus was significantly affected by the heated bed temperature, the raster angle and hotend temperature. In the previous case in which the layer fan was used, a negative effect was also observed with increasing the hotbed temperature. During the 3D-printing process, these specimens were thermally affected by the bed temperature degradati giving to somewhat annealing which resulted in lowering the stiffness. The use of a raster pattern aligned with the applied load direction, again had a positive effect on the tensile modulus. Finally, the effect of the nozzle temperature had a negative effect due to the thermal degradation as mentioned above. While 3D-printed samples with a transversal pattern and a heated bed at 60°C and the hot end at 185°C led to a tensile modulus of 614 MPa, slightly higher tensile modulus was obtained for same conditions but using a hot end temperature of 175°C (tensile modulus of about 645 MPa, thus showing a percentage increase of 4.8%).

Figure 3 shows the ANOVA analysis regarding the effects of using the layer fan or not, on tensile properties of the 3D-printed specimens. As observed, the effect of using the layer fan had a positive influence on all three tensile parameters (tensile strength, tensile modulus, elongation at break). With regard to both tensile strength and elongation at break, despite having a positive influence as the ANOVA analysis revealed, there was no significant difference between using the layer fan or not. As mentioned above, when a slow cooling process is applied to a

PHA polymer, the crystallisation is enhanced and internal stresses are generated due to the shrinkage associated to crystallisation. These internal stresses result in micro (or macro) crack formation with a negative effect on cohesion and toughness. The use of the layer fan leads to a faster cooling process which prevents from excessive crystallisation and therefore, less micro (or macro) cracks are generated. The ANOVA statistical analysis showed that the use of the layer fan had a significant effect on the tensile modulus. The tensile modulus values obtained for 3D-printed samples coded as 175-60L with the layer fan on was 846 MPa. In contrast, 3D-printed samples with the same conditions but without the layer fan showed a lower tensile modulus of 666 MPa (which stands for a percentage decrease of 21.2%), thus confirming the importance of the layer fan on final mechanical properties. When the layer fan was used, the 3D-printed layers are cooled down faster, resulting in a structure with a lower degree of crystallinity (El-Hadi et al. 2002). A lower proportion of crystalline phase implies a higher presence of amorphous phase. PHA are characterised by having a rigid amorphous phase (RAF) which has a higher stiffness, and therefore modifies the final tensile modulus of the material (Wang et al. 2016).

Regarding other works with PHA in which a FDM was employed to obtain tensile test samples, four works can be highlighted. One parameter to consider is that different types of PHA polymer can be found in the market with different mechanical properties, so it is difficult to compare the herein results with those reported by other authors. Another parameter to consider is the effect of the aging in the samples. As mentioned above, the mechanical properties of the manufactured samples highly depend on the time elapsed from manufacture until characterisation, since PHA undergo physical aging. Tian et al. employed a PHA polymer blended with wood flour and employed a micro-screw extrusion. They reported a maximum tensile strength of 40 MPa and an elongation at break of around 2.5% for the composite containing 10 wt.% wood flour load and a printing pattern of 0° (Tian et al. 2021). Wu et al. used palm fibre to manufacture filaments of PHA for 3D-printing. The tensile strength of the neat PHA 3D-printed specimens was 16.5 MPa while in other work, they reported a tensile strength of 17.4 MPa for the neat PHA 3D-printed part, and a surprisingly high elongation at break of 600% (Wu, Liao, and Cai 2017; Wu 2018). Finally, Valentini et al. manufactured filament for 3D-printing with PHBH and subsequently, they obtained tensile test specimens for further characterisation. They reported

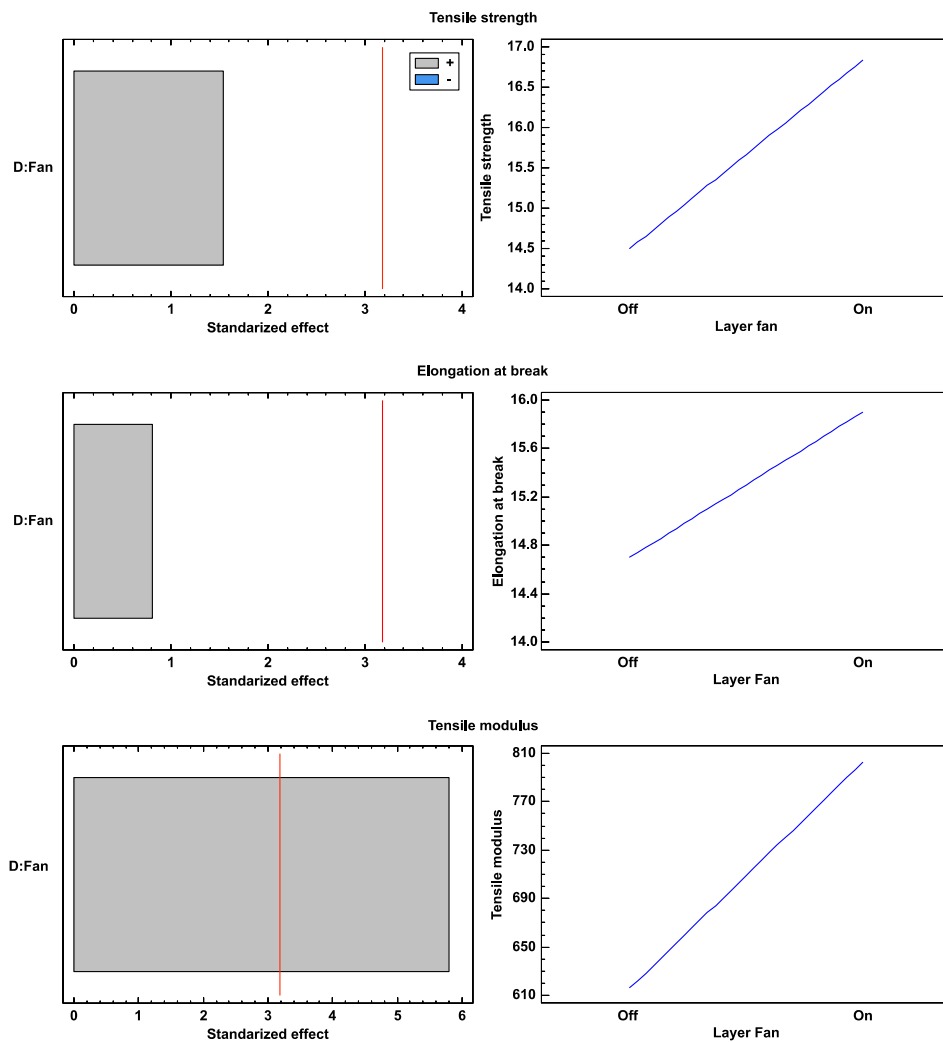


Figure 3. Summary of the ANOVA analysis for 3D-printed PHBH specimens with and without the layer fan, Pareto diagram standardised effect (left row) and the main effects diagram (right row) for tensile strength, elongation at break and tensile modulus.

a tensile strength of 21.6 MPa and an elongation at break of 10.4% for samples obtained using a raster angle of $\pm 45^\circ$ (Valentini et al. 2019).

3.2 Fracture morphology of the PHBH obtained by additive manufacturing

Figure 4 gathers some field emission scanning electron microscopy (FESEM) images of the 3D-printed PHBH specimens obtained by using a hot end at 185°C , a heated bed at 70°C and the fan layer switched on. The different conditions proposed in this work did not provide different surface morphologies due to the mechanical properties measured did not change in a wide range. Figure 4(a) shows the fracture surface of a 3D-printed specimen using a transversal raster (T), i.e. perpendicular to the applied load in the tensile test. In the fracture section, each of the raster had a direction parallel to the direction of breakage. Thus, the gap that can be

seen was caused by the printing process. In contrast, Figure 4b shows the fracture surface of a 3D-printed specimen using a longitudinal pattern (L), resulting in the hole that can be observed having a triangular geometry (0.1 mm length) due to the shape adopted by the melt polymer during the 3D-printing process. In this sense, Torrado et al. (2014) concluded that the presence of voids in the 3D-printing process was due to the deposition process of the different raster lines. In addition to the different shapes of the holes or voids formed depending on the 3D-printing direction, a clear difference also emerges in the morphology of the fracture surface. The 3D-printed specimen with a transverse raster (T) has a flat and smooth surface with no signs of plastic deformation. This type of microstructure is characterised by a separation of the raster prints giving rise to a flat surface as proposed by Torrado et al. (2016). On the other hand, if a longitudinal raster pattern (L) is used, the fracture morphology is remarkably different. In

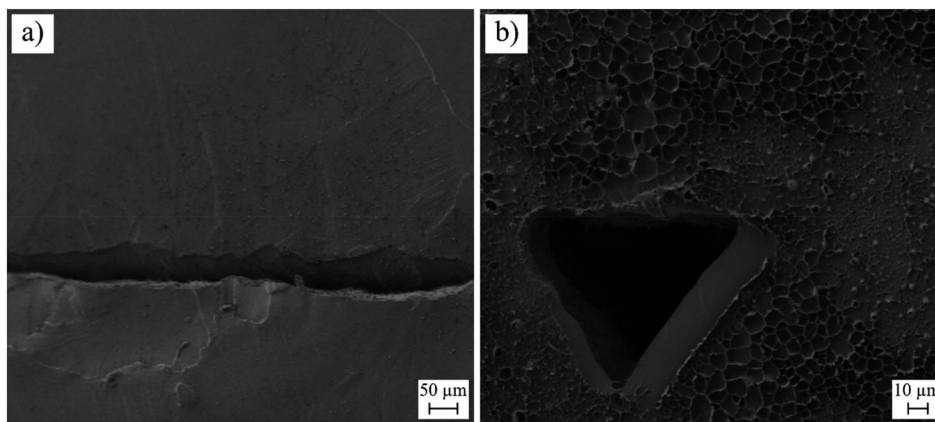


Figure 4. Fracture morphology of 3D-printed PHBH tensile specimens obtained by field emission scanning electron microscopy FESEM: (a) Image taken at 100× magnifications of a specimen 3D-printed with transversal raster (T); (b) Image taken at 200× magnifications of a specimen 3D-printed with longitudinal raster (L).

particular, it is possible to observe a rough surface as a result of the plastic deformation occurring before fracture. Quiles-Carrillo et al. and Petchwattana et al. (Petchwattana and Covavisaruch 2014; Quiles-Carrillo et al. 2018) propose that there is a relationship between the plastic deformation and the morphology of the fracture surface. A brittle fracture is characterised by a flat and smooth surface, whereas higher plastic deformation provokes higher roughness to appear. The morphologies observed on fractured surfaces are in agreement with the mechanical properties mentioned above. As it has been said previously, the specimens printed with a longitudinal pattern (L) showed higher elongation at break. On the other hand, specimens with a transverse pattern (T), the elongation at break values were lower because the fracture was governed by the adhesion between the different raster lines.

3.3 Thermal characterisation of PHBH

The main thermal properties obtained by differential scanning calorimetry (DSC) are gathered in Table 7 with the aim of assessing the effect of the annealing conditions and the cooling of PHBH on mechanical properties, while Figure 5 gathers the DSC curves obtained during the tests. To analyse the final state of the material after aging under the different processing conditions proposed, a single heating cycle from -50°C to 200°C

was scheduled. The PHBH used in this research is characterised by a glass transition temperature (T_g) close to 0°C . This parameter must be considered to select the temperature of the heated bed so that it is above to ensure the best adhesion of the 3D-printed specimens. To achieve a good adhesion, the heated bed was set above 60°C to ensure good adhesion. In these conditions, absence of warping was observed on 3D-printed parts. Contrary, it was not possible to achieve a good adhesion at lower heated bed temperatures than 60°C . The effect of temperature on the suitable heated bed conditions was studied by Spoerk et al. demonstrated that the adhesion forces to the heated bed increased above the glass transition temperature, T_g (2018). A noticeable effect after the aging process of the samples was the absence of a cold crystallisation peak, which showed that the polymer reached a stable packed structure that could no longer be modified by heat treatment. On the other hand, different melting peaks appeared due to the fact that PHBH is a semi-crystalline copolymer in which different types of crystals are formed and melt at different temperatures comprised between 108°C and 161°C . This parameter is of special interest because it allows the selection of the working temperature range. By taking into account the results obtained by DSC and bearing in mind that the onset degradation temperature must not be reached, a temperature of 175°C was selected as the minimum

Table 7. Summary of the differential scanning calorimetry (DSC) test of the samples in terms of glass transition temperature (T_g), melting temperature (T_m), melting enthalpy (H_m) and degree of crystallinity (X_c).

Code	T_g ($^{\circ}\text{C}$)	T_{m1} ($^{\circ}\text{C}$)	T_{m2} ($^{\circ}\text{C}$)	T_{m3} ($^{\circ}\text{C}$)	H_m (J/g)	X_c (%)
Pellet	0.5 ± 0.3	108.3 ± 0.2	122.0 ± 0.3	156.2 ± 0.1	35.0 ± 0.2	23.9 ± 0.2
175-60 F	0.8 ± 0.2	110.5 ± 0.1	123.2 ± 0.1	158.3 ± 0.2	38.0 ± 0.2	26.0 ± 0.1
175-70 F	1.0 ± 0.1	111.3 ± 0.3	124.7 ± 0.2	159.0 ± 0.2	39.2 ± 0.3	26.9 ± 0.2
175-80 F	0.8 ± 0.1	111.7 ± 0.2	125.2 ± 0.2	161.1 ± 0.1	40.5 ± 0.1	27.7 ± 0.1
175-60 NF	1.1 ± 0.2	111.6 ± 0.1	125.3 ± 0.1	160.6 ± 0.2	40.3 ± 0.1	27.6 ± 0.1

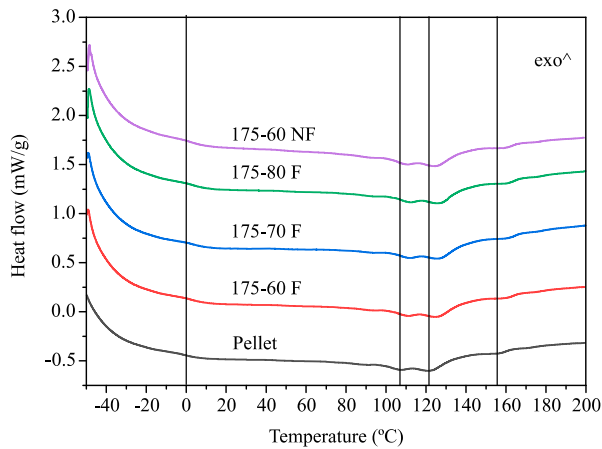


Figure 5. Summary of the DSC analysis for PHBH under different cooling conditions. Vertical lines indicate the temperatures at which the main thermal transition occur for the pellet sample.

temperature needed in the 3D-printing process, which is high enough to ensure full melting of crystallites. It is worthy to highlight the increase of the temperature at which these characteristic melting peaks were observed as a function of the processing conditions used. This shift is related to the change in the degree of crystallinity of the samples. A higher degree of crystallinity results in an increase in the perfection of the crystals so that a higher temperature is required to melt them. This effect is described by Srubar et al. work in PHB and PHBV subjected to different aging times. They observed a small increase in the melting temperatures in the characteristic DSC thermograms as the aging time increased (Srubar et al. 2012).

As proposed, an annealing process associated with the heated bed conditions used during printing had a clear effect on the degree of crystallinity of the sample which changes from 26.0% for the sample manufactured with the lowest heated bed temperature up to 27.7% for 3D-printed samples with a heated bed of 80°C. Additionally, the removal of the layer fan gave rise to a similar effect to that produced by increasing the temperature of the heated bed. In this case the cooling rate of the polymer deposited in the melt state is slower, thus allowing to reach a higher degree of crystallinity. Vitorino et al. studied the effect of the cooling rate in a PHB/babassu composites under nonisothermal conditions showing that the composite with 10 wt.% filler achieved a degree of crystallinity of 57.8% at 2°C/min and this value decreased up to 39.6% with a cooling rate of 32°C/min (2016). The thermal properties of the PHBH pellets show the behaviour of the material before being 3D-printed; this means without any thermal history related to the 3D-printing process. It is important to bear in mind that PHBH pellets are industrially subjected to fast cooling rates, so that, the degree of crystallinity of the material is lower. Consequently, the melting temperatures are reduced compared with the samples obtained from the 3D-printed samples.

Regarding the thermogravimetric behaviour of PHBH, Figure 6 shows that the onset degradation temperature is around 277°C taking as a criterion a 5% mass loss (Dong et al. 2015). Once the degradation starts, a single step mass loss occurs with a maximum degradation rate located at 309°C. With the results

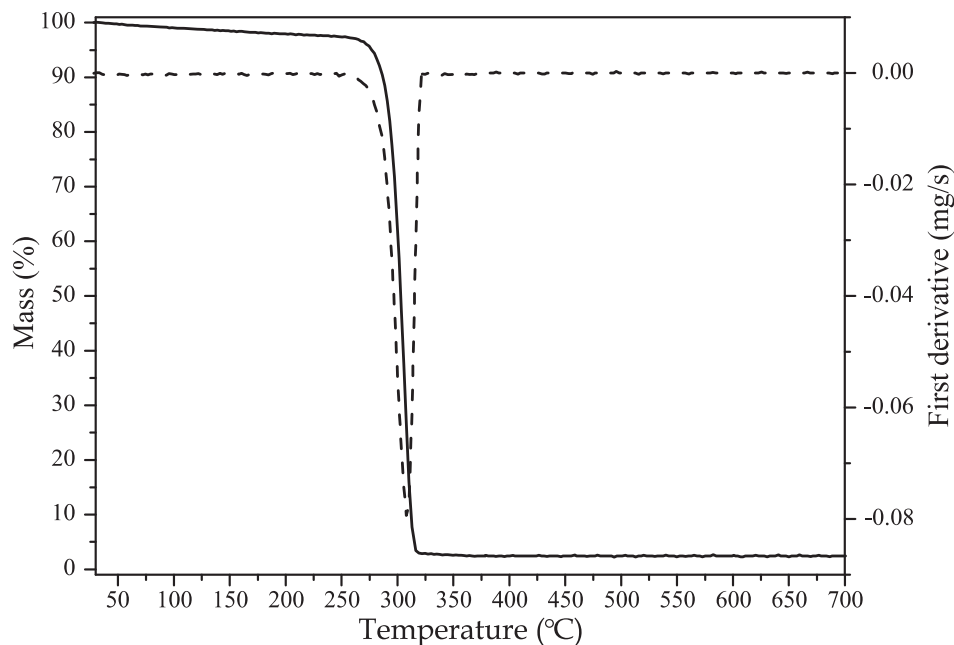


Figure 6. Summary of the TGA analysis for PHBH pellet in terms of mass loss (continuous line) and first derivative curve, DTG (dashed line).

obtained, the proposed working temperatures fall within the processing window of PHBH and hence, this range avoids severe thermal degradation on PHBH. Despite of this, a decrease in the mechanical properties is observed by increasing the working temperature due the chain scission of PHBH as reported by other authors, even working at temperatures lower than the onset degradation temperatures, which is a typical drawback when working with polyhydroxyalkanoates (Shojaeiarani et al. 2019).

3.4 Printability of PHBH

One of the main drawbacks when using PHBH by additive manufacturing is the difficulty in achieving good adhesion of the 3D-printed part to the heated bed due to the shrinkage related to fast crystallisation as it has been aforementioned. At first, an attempt was made with the bed at room temperature as in many other polymers used in 3D-printing. This was made to check 3D-printability in these usual conditions since the heated bed includes a new variable to the process. In this case, the first layer did not obtain a good adhesion. Due to this poor adhesion, a search for the minimum heated bed temperature to achieve good adhesion on the first layer was carried out. This minimum temperature was 60°C; below this threshold, the adhesion of the first layer was poor and, subsequently, the 3D-printing process was not possible. Above this temperature threshold, adhesion is good enough to guarantee the 3D-printing process.

After overcoming the previously mentioned drawback, a second problem arose. This was related to the physical aging of PHA at room temperature which leads to secondary crystallisation which, in turn, leads to an additional shrinkage that could potentially compromise the 3D-printing process, mainly due to undesired warping. This phenomenon affecting PHA was analysed by Chan et al. for PHBV (2018). In order to ensure the adhesion of 3D-printed parts to the heated bed, a 4 mm brim around the shape was included in the gcode. This allowed good adhesion during all the 3D-printing process, thus preventing it from detachment. Despite considering all these issues, some of the combinations scheduled in the design of experiments resulted in some undesired warping, and the corresponding 3D-printing process was stopped. Additionally, when the heated bed temperature was set above 80°C, some additional warping appeared, thus establishing 80°C as the upper temperature threshold for PHBH processing by 3D-printing. Usually, the polymer-bed adhesion improves by increasing the heated bed temperature, as in the case of ABS. This phenomenon is even much pronounced above the glass transition

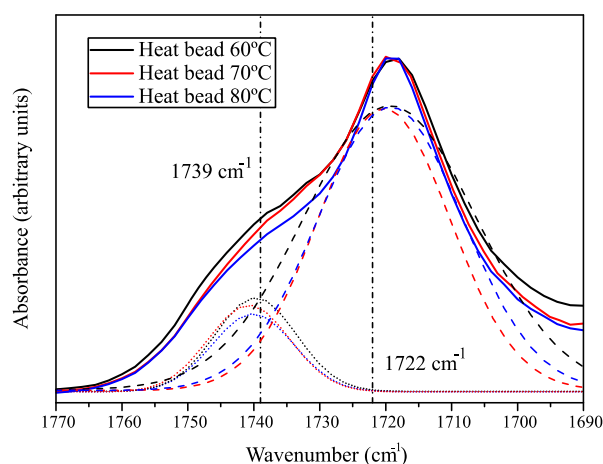


Figure 7. Comparison of the normalised Fourier-transform infrared spectroscopy (FTIR) spectra in the 1770–1690 cm^{-1} range, for 3D-printed specimens with different heated bead temperatures, a constant hotend of 175°C, and the layer fan switched on. Deconvoluted peaks are indicated in dashed lines.

temperature of the polymer. Above T_g , the polymer achieves a higher chain mobility, thus improving the adhesion to the bed (Spoerk et al. 2018). Under high heated bed temperatures, PHBH crystallisation was enhanced, and hence a higher shrinkage was obtained, so that the warping phenomena was more noticeable.

In the case of PHBH, similar to other PHAs, the adhesion strength to the bed is also linked to the degree of crystallinity that the samples acquire. This can be estimated by using infrared spectroscopy as proposed by Kansiz et al. (2007), in PHA. The 1739 cm^{-1} band is usually assigned to the amorphous domain while the 1722 cm^{-1} band corresponds to the crystalline phase. Depending on the prominence of each one of these characteristic bands, the degree of crystallinity of a sample can be compared qualitatively. In this case, changes in these bands when the temperature of the heated bed was modified, was collected by FTIR and the results are shown in Figure 7, which also includes the deconvoluted peaks.

For the different temperatures considered, it can be seen that the higher the heated bed temperature, the absorption of the band associated with the amorphous part decreases, the deconvoluted peak obtained at 1722 cm^{-1} was also reduced. This indicates that PHBH has reached a higher degree of crystallinity. As a result, samples have higher shrinkage, giving rise to warping problems above 80°C. These results agree with those reported by Gopi et al. (2018). They concluded that the degree of crystallinity acquired by the sample is clearly influenced by the cooling conditions which a key parameter in 3D-printing. They also reported an increase in crystallinity on PHA after isothermal crystallisation

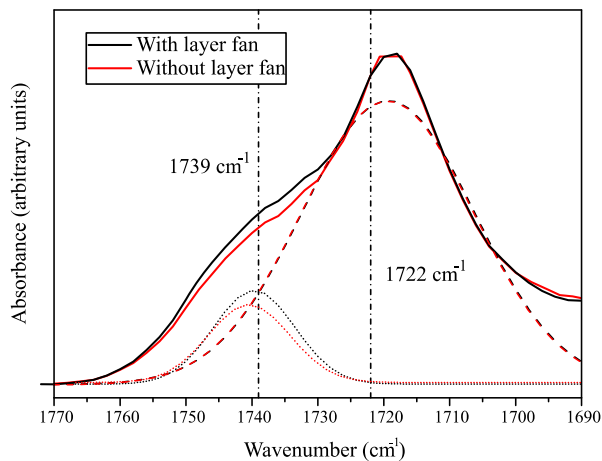


Figure 8. Comparison of the normalised Fourier-transform infrared spectroscopy (FTIR) spectra in the 1770–1690 cm^{-1} range, for different samples 3D-printed at 175°C hotend and 60°C heated bed with and without layer fan. Deconvoluted peaks are indicated in dashed lines.

(or annealing). The degree of crystallisation was higher as the annealing temperature increased. This effect could also be observed in the DSC characterisation analysis mentioned above.

In addition to the heated bed temperature, there is also a parameter that plays a key role in the cooling process. It is the use (or not) of the layer fan. When layer fan is switched on during the 3D-printing process, the melt polymer through the nozzle cools down quickly in order to obtain a higher print quality. In the work of Xie et al. (2008), the effect of cooling rates on different PHA was analysed. In all cases, a higher degree of crystallinity was achieved at slow cooling rates.

As mentioned above, when a higher degree of crystallinity was reached, the dimensional shrinkage was more pronounced leading to warping at heated bed temperatures above 70°C (without layer fan) thus limiting the processing range. This phenomenon can be seen in Figure 8. In this case, FTIR spectra with a constant nozzle temperature of 175°C and a heated bed of 60°C were compared depending on the use or not of the layer fan. When the layer fan is switched off, a higher degree of crystallinity was acquired by PHBH as one can see, the deconvoluted peak of the amorphous region had lower intensity.

Finally, the temperatures at which PHBH could be processed ranged from 175°C to 185°C in the heat zone 1. At lower temperatures, the stepper motor was not able to achieve continuous screw rotation and, therefore, the extrusion of the material was not uniform. As observed in the DSC study, the highest melting peak observed on PHBH is around 165°C, so

the minimum working temperature was set as 175°C to ensure that the polymer is completely melted. The maximum temperature at which it was possible to process PHBH was limited by the jam formation. Above 185°C, the heat zone 2 exceeded 104°C due to heat transmission along the screw. The used PHBH had a broad melting range with the onset located at around 100°C. To prevent jam formation, a single-screw equipment requires the material to be in a solid state in the initial zone and then melt progressively along the screw (Liu et al. 2019). Another parameter to consider is the thermogravimetric analysis that shows the mass loss with increasing temperature. In a previous work we observed that PHBH starts the mass loss at 277°C, so the proposed working temperatures avoid severe thermal degradation phenomenon on PHBH (Ivorra-Martinez et al. 2020a). Despite working below the onset degradation temperatures, PHBH, as other aliphatic polyesters, can undergo chain scission in each thermal cycle, which in turn, leads to a slight decrease in the molecular weight (Shojaeiarani et al. 2019).

3.5 Visual appearance of the PHBH 3D-printed parts

In Figure 9, an example of some of the PHBH 3D-printed parts can be seen. It includes examples of the specimens used for mechanical characterisation, with both types of patterns used in the longitudinal (L) and transverse (T) directions. In addition, these incorporate the necessary brim to achieve the correct manufacturing process and avoid detachment.

Moreover, other more complex shapes were 3D-printed to assess the printability of PHBH. In general, the visual appearance of the 3D-printed parts was satisfactory. It should be noted that no retraction movements have been used because the 3D-printer equipped with the single-screw, allow direct work with pellets, but it does not deal with this type of movement properly. Despite this, there has been no significant stringing as it can be seen in the benchy.

Regarding the level of detail, in any case is not very high, because the configuration used is the same as that of the test specimens, in which a layer height of 0.4 mm and a line width of 0.8 mm was used.

4 Conclusions

The effect of different 3D-printing parameters for additive manufacturing with PHBH were analysed. Due to the high sensitiveness of PHBH to thermal degradation during processing as a result of presenting a very



Figure 9. Examples of the PHBH 3D-printed parts: (a) dog bone samples with both infills; (b) pencil pot; (c) benchy and a calibration cube.

narrow processing window, this work has concluded it is possible to 3D-print high quality parts without filament, by using a 3D-printer with a coupled single screw extruder fed with PHBH pellets. The most relevant parameter having a remarkable effect on mechanical properties is the raster angle. As expected, the best results were obtained for those samples manufactured with a longitudinal raster pattern (L) aligned with the applied loading direction in the tensile test. Regarding the temperature ranges, the hot end allowed to improve the beads adhesion that improved the mechanical performance, but above 180°C this effect disappeared due to the thermal degradation of the polymer. The effect of the heated bed temperature was linked with the layer fan used for the cooling. Under slow cooling conditions, the mechanical properties were rather poor due to a higher degree of crystallinity achieved that typically promotes crack formation in the internal structure. Changes in the internal structure of the samples were observed by Fourier-transform infrared spectroscopy (FTIR) showing that the modification of the printing parameters had an effect in the polymer internal structure that promoted the differences in the mechanical properties. As it has been shown in this work, the effect of the working temperatures and cooling conditions play a key role during the manufacturing process. In future works with PHA in 3D-printing, these parameters must be considered as relevant to assess the desired final properties.

Acknowledgements

Microscopy services of the Universitat Politècnica de València (UPV) are acknowledged for their help in collecting and analysing the FESEM images.

Disclosure statement

No potential conflict of interest was reported by the author(s).

Funding

This research is a part of the grant PID2020-116496RB-C22 funded by MCIN/AEI/10.13039/501100011033. Authors also thank Generalitat Valenciana-GVA for funding this research through the grant numbers AICO/2021/025 and CIGE/2021/094. Wants to thank the Ministerio de Ciencia e Innovación and Universities for his FPU grant (FPU19/01759). Wants to thank Generalitat Valenciana-GVA, for his FPI grant (ACIF/2021/185) and grant FPU20/01732 funded by MCIN/AEI/10.13039/501100011033 and by ESF Investing in your future. Funding for open access charge: Universitat Politècnica de València.

Notes on Contributors

Mr Ivorra-Martinez is a predoctoral student at the Universitat Politècnica de València (UPV) in the Department of Mechanical and Materials Engineering. He is also a member of the Institute of Materials Technology (ITM). He holds a degree in Mechanical Engineering from the Universitat Politècnica de València and also obtained a Master's in Mechanical Engineering and a Master's in Materials Engineering, Processing and Characterization of Materials. He is currently part of the PhD program in

Industrial Engineering and Production in which he is developing his doctoral thesis entitled “Development and characterization of industrial formulations of aliphatic polyesters for injection and additive manufacturing”. The research carried out focuses on the development of new polymeric materials with a low environmental impact, focusing especially on their processing by means of different manufacturing techniques such injection molding and additive manufacturing.

Dr. Peydró-Rasero has 30 years of experience in the design and manufacture of plastic injection molds, as well as in the handling of all machine tools (conventional and CNC). On the other hand, she is also an expert in the manufacture of plastic parts by injection or extrusion. His teaching activity has been focused on this aspect for the last 25 years, teaching subjects related to Mechanical Technology: Manufacturing Process Engineering, Industrial Processes, Flexible Manufacturing Systems, etc. He has published 9 full books, 3 book chapters, 12 conference papers, 1 journal article. His research activity has focused mainly on the study of polymers. He has participated in 6 public projects and 4 projects with companies. He has participated in the publication of 54 articles in journals (of which 12 articles are in international journals indexed in the Journal Citation Reports (JCR), most of them with high impact index). He has participated in the publication of 1 full-length books, 27 book chapters, 117 conference papers. He has been a member of journal editing committees 9 times, a member of scientific congress committees once and a member of congress organizing committees once.

Mr Gomez-Caturla is a predoctoral student at the Universitat Politècnica de València (UPV) in the Department of Mechanical and Materials Engineering. He holds a degree in Chemical Engineering from the Universitat Politècnica de València which he completed in 2019. He completed the master's degree in Engineering, Processing and Characterization of Materials at the Universitat Politècnica de València, finishing the master's degree in 2021. In March 2021 he started his contract as an FPI grant holder at the UPV, then he was awarded the FPI grant from the GVA in October 2021, and in November 2021 he obtained the FPU grant from the Ministry, a contract under which he is currently working at the UPV at the Alcoy campus as research staff and carrying out teaching collaboration tasks. His field of work is polymeric materials, more specifically combinations of polymers with waste from the agri-food industry following the principles of the circular economy.

Dra Sanchez-Nacher has more than 20 years of experience in the field of polymeric materials and polymer matrix composites. She is currently at Universitat Politècnica de València (UPV) as a Full Professor at the Alcoy Campus. She is part of the researching group Formulations and Processing and Surface Modification of Polymeric Materials Research Group - GiProSup at the UPV Institute of Materials Technology. She is co-author of more than 70 research journal publication and supervised 8 doctoral theses. Her research field is focused in the development of new biobased materials and polymer composites to try to reduce the impact of the actual polymeric materials. To this effect different manufacturing techniques as well as different modification process have been employed.

Dr. Boronat has more than 20 years of experience in the field of manufacturing processes, especially in polymeric materials and polymer matrix composites. He is currently at Universitat

Politécnica de València (UPV), where he holds the rank of Full Professor and Chair of the Mechanical and Materials Engineering Department at the Alcoy Campus. From 2017, Dr. Boronat has provided leadership at the Formulations and Processing of Polymeric Materials Research Group at the UPV Institute of Materials Technology. Dr. Boronat is a Fellow of the Manufacturing Engineering Society. He currently serves as Editor-in-Chief of the Journal of Applied Research in Technology & Engineering. Dr. Boronat has served as guest editorships including Materials journal special issue on “Environmentally Friendly Polymers and Polymer Composites” and “Advanced Materials in Additive Manufacturing for Medical Applications” and Polymers journal special issue on “Advances in Manu.

ORCID

Juan Ivorra-Martinez  <http://orcid.org/0000-0001-8968-4899>
 Miguel Ángel Peydro  <http://orcid.org/0000-0002-8503-1505>
 Jaume Gomez-Caturla  <http://orcid.org/0000-0001-8680-4509>
 Teodomiro Boronat  <http://orcid.org/0000-0002-2144-2874>
 Rafael Balart  <http://orcid.org/0000-0001-5670-7126>

References

- Alafaghani, A., A. Qattawi, B. Alrawi, and A. Guzman. 2017. “Experimental Optimization of Fused Deposition Modelling Processing Parameters: A Design-for-Manufacturing Approach.” *Procedia Manufacturing* 10: 791–803. doi:10.1016/j.promfg.2017.07.079
- Algarni, M. 2021. “The Influence of Raster Angle and Moisture Content on the Mechanical Properties of PLA Parts Produced by Fused Deposition Modeling.” *Polymers* 13 (2): 1–12. doi:10.3390/polym13020237
- Anjum, A., M. Zuber, K. M. Zia, A. Noreen, and S. Tabasum. 2016. “Microbial Production of Polyhydroxyalkanoates (PHAs) and its Copolymers: A Review of Recent Advancements.” *International Journal of Biological Macromolecules* 89: 161–174. doi:10.1016/j.ijbiomac.2016.04.069
- Ayatollahi, M. R., A. Nabavi-Kivi, B. Bahrami, M. Yazid Yahya, and M. R. Khosravani. 2020. “The Influence of In-Plane Raster Angle on Tensile and Fracture Strengths of 3D-Printed PLA Specimens.” *Engineering Fracture Mechanics* 237, 107225. doi:10.1016/j.engfracmech.2020.107225
- Bermudez, D., P. A. Quiñonez, E. J. Vasquez, I. ACarrete, T. J. Word, and D. A. Roberson. 2021. “A Comparison of the Physical Properties of two Commercial 3D Printing PLA Grades.” *Virtual and Physical Prototyping* 16 (2): 178–195. doi:10.1080/17452759.2021.1910047
- Bordes, P., E. Pollet, S. Bourbigot, and L. Avérous. 2008. “Structure and Properties of PHA/Clay Nano-Biocomposites Prepared by Melt Intercalation.” *Macromolecular Chemistry and Physics* 209 (14): 1473–1484. doi:10.1002/macp.200800022
- Chan, C. M., L.-J. Vandí, S. Pratt, P. Halley, D. Richardson, A. Werker, and B. Laycock. 2018. “Mechanical Performance and Long-Term Indoor Stability of Polyhydroxyalkanoate (PHA)-Based Wood Plastic Composites (WPCs) Modified by Non-Reactive Additives.” *European Polymer Journal* 98: 337–346. doi:10.1016/j.eurpolymj.2017.11.041
- Chen, L., R. Mao, L. Zhang, J. Xu, D. Li, J. Bao, and Z. Wang 2021. “Dramatic Toughness Improvement of Poly(3-

- Hydroxybutyrate-co-3-Hydroxyvalerate) by Supercritical Carbon Dioxide-Assisted Annealing." *Polymers for Advanced Technologies* 32 (9): 3646–3654. doi:10.1002/pat.5373
- Cherpinski, A., S. Torres-Giner, L. Cabedo, and J. M. Lagaron. 2017. "Post-processing Optimization of Electrospun Submicron Poly(3-Hydroxybutyrate) Fibers to Obtain Continuous Films of Interest in Food Packaging Applications." *Food Additives & Contaminants Part A: Chemistry, Analysis, Control, Exposure & Risk Assessment* 34 (10): 1817–1830. doi:10.1080/19440049.2017.1355115
- Crump, S. S. 1989. *Inventor Apparatus and Method for Creating Three-Dimensional Objects*. United States.
- Dave, H. K., N. H. Patadiya, A. R. Prajapati, and S. R. Rajpurohit. 2021. "Effect of Infill Pattern and Infill Density at Varying Part Orientation on Tensile Properties of Fused Deposition Modeling-Printed Poly-Lactic Acid Part." *Proceedings of the Institution of Mechanical Engineers Part C Journal of Mechanical Engineering Science* 235 (10): 1811–1827. doi:10.1177/0954406219856383
- Diederichs, E. V., M. C. Picard, B. P. Chang, M. Misram, D. F. Mielewski, A. K. Mohanty. 2019. "Strategy to Improve Printability of Renewable Resource-Based Engineering Plastic Tailored for fdm Applications." *ACS Omega* 4 (23): 20297–20307. doi:10.1021/acsomega.9b02795
- Dizon, J. R. C., A. H. Espera, Q. Chen, and R. C. Advincula. 2018. "Mechanical Characterization of 3D-Printed Polymers." *Additive Manufacturing* 20: 44–67. doi:10.1016/j.addma.2017.12.002
- Dong, Y., J. Marshall, H. J. Haroosh, S. Mohammadzadehmoghadam, D. Liu, X. Qi, and K.-T. Lau. 2015. "Polylactic Acid (PLA)/Halloysite Nanotube (HNT) Composite Mats: Influence of HNT Content and Modification." *Composites Part A: Applied Science and Manufacturing* 76: 28–36. doi:10.1016/j.compositesa.2015.05.011
- Dudescu, C., and L. Racz. 2017. "Effects of Raster Orientation, Infill Rate and Infill Pattern on the Mechanical Properties of 3D Printed Materials." *Acta Universitatis Cibiniensis Technical Series*. 69 (1): 23–30. doi:10.1515/aucts-2017-0004
- El-Hadi, A., R. Schnabel, E. Straube, G. Müller, and S. Henning. 2002. "Correlation Between Degree of Crystallinity, Morphology, Glass Temperature, Mechanical Properties and Biodegradation of Poly (3-Hydroxyalkanoate) PHAs and Their Blends." *Polymer Testing* 21 (6): 665–674. doi:10.1016/S0142-9418(01)00142-8
- Gardan, J. 2019. "Smart Materials in Additive Manufacturing: State of the art and Trends." *Virtual and Physical Prototyping* 14 (1): 1–18. doi:10.1080/17452759.2018.1518016
- Gonzalez-Gutierrez, J., S. Cano, S. Schuschnigg, C. Kukla, J. Sapkota, and C. Holzer. 2018. "Additive Manufacturing of Metallic and Ceramic Components by the Material Extrusion of Highly-Filled Polymers: A Review and Future Perspectives." *Materials* 11 (5): 840. doi:10.3390/ma11050840
- Gopi, S., M. Kontopoulou, B. A. Ramsay, and J. A. Ramsay. 2018. "Manipulating the Structure of Medium-Chain-Length Polyhydroxyalkanoate (MCL-PHA) to Enhance Thermal Properties and Crystallization Kinetics." *International Journal of Biological Macromolecules* 119: 1248–1255. doi:10.1016/j.ijbiomac.2018.08.016
- Hull, C. W. 1998. "Inventor Method for Production of Three-Dimensional Objects by Stereolithography." United States.
- Ivorra-Martinez, J., J. Manuel-Mañogil, T. Boronat, L. Sanchez-Nacher, R. Balart and L. Quiles-Carrillo. 2020a. "Development and Characterization of Sustainable Composites from Bacterial Polyester Poly(3-Hydroxybutyrate-co-3-Hydroxyhexanoate) and Almond Shell Flour by Reactive Extrusion with Oligomers of Lactic Acid." *Polymers* 12 (5): 1097. doi:10.3390/polym12051097
- Ivorra-Martinez, J., I. Verdu, O. Fenollar, L. Sanchez-Nacher, R. Balart, and L. Quiles-Carrillo. 2020b. "Manufacturing and Properties of Binary Blend from Bacterial Polyester Poly(3-Hydroxybutyrate-co-3-Hydroxyhexanoate) and Poly (Caprolactone) with Improved Toughness." *Polymers* 12 (5): 1118. doi:10.3390/polym12051118
- Kabe, T., C. Hongo, T. Tanaka, T. Hikima, M. Takata, and T. Iwata. 2015. "High Tensile Strength Fiber of Poly[(R)-3-Hydroxybutyrate-co-(R)-3-Hydroxyhexanoate] Processed by two-Step Drawing with Intermediate Annealing." *Journal of Applied Polymer Science* 132 (2): 41258–41265. doi:10.1002/app.41258
- Kabe, T., T. Tsuge, K. I. Kasuya, A. Takemura, T. Hikima, M. Takata, and T. Iwata. 2012. "Physical and Structural Effects of Adding Ultrahigh-Molecular-Weight Poly[(R)-3-Hydroxybutyrate] to Wild-Type Poly[(R)-3-Hydroxybutyrate]." *Macromolecules* 45 (4): 1858–1865. doi:10.1021/ma202285c
- Kansiz, M., A. Domínguez-Vidal, D. McNaughton, and B. Lendl. 2007. "Fourier-transform Infrared (FTIR) Spectroscopy for Monitoring and Determining the Degree of Crystallisation of Polyhydroxyalkanoates (PHAs)." *Analytical and Bioanalytical Chemistry* 388 (5-6): 1207–1213. doi:10.1007/s00216-007-1337-5
- Kovalcik, A. 2021. "Recent Advances in 3D Printing of Polyhydroxyalkanoates: A Review." *The EuroBiotech Journal* 5 (1): 48–55. doi:10.2478/ebtj-2021-0008
- Kovalcik, A., L. Sangroniz, M. Kalina, K. Skopalova, P. Humpolíček, M. Omastova, N. Mundigler, and A. J. Müller. 2020. "Properties of Scaffolds Prepared by Fused Deposition Modeling of Poly(Hydroxyalkanoates)." *International Journal of Biological Macromolecules* 161: 364–376. doi:10.1016/j.ijbiomac.2020.06.022
- Kumar, R., M. Kumar, and J. S. Chohan. 2021. "The Role of Additive Manufacturing for Biomedical Applications: A Critical Review." *Journal of Manufacturing Processes* 64: 828–850. doi:10.1016/j.jmapro.2021.02.022
- Kurusu, R. S., N. R. Demarquette, C. Gauthier, and J.-M. Chenal. 2014. "Effect of Ageing and Annealing on the Mechanical Behaviour and Biodegradability of a Poly(3-Hydroxybutyrate) and Poly(Ethylene-co-Methyl-Acrylate-co-Glycidyl-Methacrylate)Blend." *Polymer International* 63 (6): 1085–1093. doi:10.1002/pi.4616
- Kurusu, R. S., C. A. Siliki, T. David, N. R. Demarquette, C. Gauthier, and J.-M. Chenal. 2015. "Incorporation of Plasticizers in Sugarcane-Based Poly(3-Hydroxybutyrate)(PHB): Changes in Microstructure and Properties Through Ageing and Annealing [Article]." *Industrial Crops and Products* 72: 166–174. doi:10.1016/j.indcrop.2014.12.040
- Laycock, B., P. Halley, S. Pratt, A. Werker, and P. Lant. 2014. "The Chemomechanical Properties of Microbial

- Polyhydroxyalkanoates." *Progress in Polymer Science* 39 (2): 397–442. doi:10.1016/j.progpolymsci.2013.06.008
- Liu, T., X. Tian, Y. Zhang, Y. Cao, and D. Li. 2020. "High-pressure Interfacial Impregnation by Micro-Screw in-Situ Extrusion for 3D Printed Continuous Carbon Fiber Reinforced Nylon Composites." *Composites Part A: Applied Science and Manufacturing* 130: 105770. doi:10.1016/j.compositesa.2020.105770
- Liu, G., Y. Xiong, and L. Zhou. 2021. "Additive Manufacturing of Continuous Fiber Reinforced Polymer Composites: Design Opportunities and Novel Applications." *Composites Communications* 27: 100907. doi:10.1016/j.coco.2021.100907
- Liu, S., P. Zhao, S. Wu, C. Zhang, J. Fu, and Z. Chen. 2019. "A Pellet 3D Printer: Device Design and Process Parameters Optimization." *Advances in Polymer Technology* 2019: 5075327. doi:10.1155/2019/5075327
- Mahmood, H., A. Pegoretti, R. S. Brusa, R. Ceccato, L. Penasa, S. Tarter, and R. Checchetto. 2020. "Molecular Transport Through 3-Hydroxybutyrate co-3-Hydroxyhexanoate Biopolymer Films with Dispersed Graphene Oxide Nanoparticles: Gas Barrier, Structural and Mechanical Properties." *Polymer Testing* 81: 106181. doi:10.1016/j.polymertesting.2019.106181
- Menčík, P., R. Příklad, I. Stehnová, V. Melčová, S. Kontárová, S. Figalla, P. Alexy, and J. Bočkaj. 2018. "Effect of Selected Commercial Plasticizers on Mechanical, Thermal, and Morphological Properties of Poly(3-Hydroxybutyrate)/Poly(Lactic Acid)/Plasticizer Biodegradable Blends for Three-Dimensional (3D) Print." *Materials* 11 (10), 1893. doi:10.3390/ma11101893
- Morales, M. A., C. L. Atencio Martinez, A. Maranon, C. Hernandez, V. Michaud and A. Porras. 2021. "Development and Characterization of Rice Husk and Recycled Polypropylene Composite Filaments for 3d Printing." *Polymers* 13 (7). doi:10.3390/polym13071067
- Pappas, J. M., A. R. Thakur, M. C. Leu, and X. Dong. 2021. "A Comparative Study of Pellet-Based Extrusion Deposition of Short, Long, and Continuous Carbon Fiber-Reinforced Polymer Composites for Large-Scale Additive Manufacturing." *Journal of Manufacturing Science and Engineering* 143 (7): 071012–071024. doi:10.1115/1.4049646
- Pereira, T., M. Silva, M. Oliveira, I. A. Maiam, M. F. Costa, R. M. S. M. Thiré. 2012. "Effect of Process Parameters on the Properties of Selective Laser Sintered Poly (3-Hydroxybutyrate) Scaffolds for Bone Tissue Engineering." *Virtual and Physical Prototyping* 7 (4): 275–285. doi:10.1080/17452759.2012.738551
- Petchwattana, N., and S. Covavisaruch. 2014. "Mechanical and Morphological Properties of Wood Plastic Biocomposites Prepared from Toughened Poly(Lactic Acid) and Rubber Wood Sawdust (Hevea Brasiliensis)." *Journal of Bionic Engineering* 11 (4): 630–637. doi:10.1016/S1672-6529(14)60074-3
- Quiles-Carrillo, L., S. Duarte, N. Montanes, S. Torres-Giner, and R. Balart. 2018. "Enhancement of the Mechanical and Thermal Properties of Injection-Molded Polylactide Parts by the Addition of Acrylated Epoxidized Soybean Oil." *Materials and Design* 140: 54–63. doi:10.1016/j.matdes.2017.11.031
- Rajpurohit, S. R., and H. K. Dave. 2018. "Effect of Process Parameters on Tensile Strength of FDM Printed PLA Part." *Rapid Prototyping Journal* 24 (8): 1317–1324. doi:10.1108/RPJ-06-2017-0134
- Relinque, J. J., A. S. de León, J. Hernández-Saz, M. G. García-Romero, F. J. Navas-Martos, G. Morales-Cid and S. I. Molina. 2019. "Development of Surface-Coated Poly(lactic Acid)/Polyhydroxyalkanoate (PLA/PHA) Nanocomposites." *Polymers* 11 (3). doi:10.3390/polym11030400
- Rodríguez-Panes, A., J. Claver, and A. M. Camacho. 2018. "The Influence of Manufacturing Parameters on the Mechanical Behaviour of PLA and ABS Pieces Manufactured by FDM: A Comparative Analysis." *Materials* 11 (8), 1333. doi:10.3390/ma11081333
- Safari, S., and T. G. M. van de Ven. 2015. "Effect of Crystallization Conditions on the Physical Properties of a two-Layer Glassine Paper/Polyhydroxybutyrate Structure." *Journal of Materials Science* 50 (10): 3686–3696. doi:10.1007/s10853-015-8929-9
- Shojaeiarani, J., D. S. Bajwa, C. Rehovsky, and G. Vahidi. 2019. "Deterioration in the Physico-Mechanical and Thermal Properties of Biopolymers Due to Reprocessing." *Polymers* 11 (1): 58. doi:10.3390/polym11010058
- Singamneni, S., D. Smith, M. J. LeGuen, and D. Truong. 2018. "Extrusion 3D Printing of Polybutyrate-Adipate-Terephthalate-Polymer Composites in the Pellet Form." *Polymers* 10 (8). doi:10.3390/polym10080922
- Singh, K. 2018. "Experimental Study to Prevent the Warping of 3D Models in Fused Deposition Modeling." *International Journal of Plastics Technology* 22 (1): 177–184. doi:10.1007/s12588-018-9206-y
- Singh, M., and S. Jonnalagadda. 2020. "Advances in Bioprinting Using Additive Manufacturing." *European Journal of Pharmaceutical Sciences* 143, 105167. doi:10.1016/j.ejps.2019.105167
- Singh, S., G. Singh, C. Prakash, and S. Ramakrishna. 2020. "Current Status and Future Directions of Fused Filament Fabrication." *Journal of Manufacturing Processes* 55: 288–306. doi:10.1016/j.jmapro.2020.04.049
- Solomon, I. J., P. Sevel, and J. Gunasekaran. 2020. "A Review on the Various Processing Parameters in FDM." *International Conference on Newer trends and Innovations in Mechanical Engineering, ICONTIME 2020; Elsevier Ltd; Part 2*.
- Spoerk, M., J. Gonzalez-Gutierrez, J. Sapkota, S. Schuschnigg, and C. Holzer. 2018. "Effect of the Printing bed Temperature on the Adhesion of Parts Produced by Fused Filament Fabrication." *Plastics, Rubber and Composites* 47 (1): 17–24. doi:10.1080/14658011.2017.1399531
- Spoerk, M., C. Holzer, and J. Gonzalez-Gutierrez. 2020. "Material Extrusion-Based Additive Manufacturing of Polypropylene: A Review on how to Improve Dimensional Inaccuracy and Warpage." *Journal of Applied Polymer Science* 137 (12): 48545. doi:10.1002/app.48545
- Srubar III W., Z. Wright, A. Tsui, A. T. Michel, S. L. Billington, and C. W. Frank. Characterizing the Effects of Ambient Aging on the Mechanical and Physical Properties of Two Commercially Available Bacterial Thermoplastics. *Polymer Degradation and Stability*. 2012;97(10):1922-1929. doi:10.1016/j.polymdegradstab.2012.04.011
- Tian, J., R. Zhang, Y. Wu, and P. Xue. 2021. "Additive Manufacturing of Wood Flour/Polyhydroxyalkanoates (PHA) Fully Bio-Based Composites Based on Micro-Screw Extrusion System." *Materials & Design* 199: 109418. doi:10.1016/j.matdes.2020.109418
- Torrado, A. R., and D. A. Roberson. 2016. "Failure Analysis and Anisotropy Evaluation of 3D-Printed Tensile Test

- Specimens of Different Geometries and Print Raster Patterns." *Journal of Failure Analysis and Prevention* 16 (1): 154–164. doi:10.1007/s11668-016-0067-4
- Torrado Perez, A. R., D. A. Roberson, and R. B. Wicker. 2014. "Fracture Surface Analysis of 3D-Printed Tensile Specimens of Novel ABS-Based Materials." *Journal of Failure Analysis and Prevention* 14 (3): 343–353. doi:10.1007/s11668-014-9803-9
- Valentini, F., A. Dorigato, D. Rigotti, and A. Pegoretti. 2019. "Polyhydroxyalkanoates/Fibrillated Nanocellulose Composites for Additive Manufacturing." *Journal of Polymers and the Environment* 27 (6): 1333–1341. doi:10.1007/s10924-019-01429-8
- Vitorino, M. B. C., P. B. Cipriano, R. M. R. Wellen, E. L. Canedo and L. H. Carvalho. 2016. "Nonisothermal Melt Crystallization of PHB/Babassu Compounds." *Journal of Thermal Analysis and Calorimetry* 126 (2): 755–769. doi:10.1007/s10973-016-5514-7
- Wang, S., W. Chen, H. Xiang, J. Yang, Z. Zhou and M. Zhu. 2016. "Modification and Potential Application of Short-Chain-Length Polyhydroxyalkanoate (SCL-PHA)." *Polymers* 8 (8). doi:10.3390/polym8080273
- Wu, C.-S. 2018. "Characterization,; Functionality and Application of Siliceous Sponge Spicules Additive-Based Manufacturing Biopolymer Composites." *Additive Manufacturing* 22: 13–20. doi:10.1016/j.addma.2018.04.034
- Wu, C.-S., H.-T. Liao, and Y.-X. Cai. 2017. "Characterisation,; Biodegradability and Application of Palm Fibre-Reinforced Polyhydroxyalkanoate Composites." *Polymer Degradation and Stability* 140: 55–63. doi:10.1016/j.polymdegradstab.2017.04.016
- Xie, Y., I. Noda, and Y. A. Akpalu. 2008. "Influence of Cooling Rate on the Thermal Behavior and Solid-State Morphologies of Polyhydroxyalkanoates." *Journal of Applied Polymer Science* 109 (4): 2259–2268. doi:10.1002/app.28278
- Xu, P., Y. Cao, P. Lv, P. Ma, W. Dong, H. Bai, W. Wang, M. Du, and M. Chen. 2018. "Enhanced Crystallization Kinetics of Bacterially Synthesized Poly(3-Hydroxybutyrate-co-3-Hydroxyhexanoate) with Structural Optimization of Oxalamide Compounds as Nucleators." *Polymer Degradation and Stability* 154: 170–176. doi:10.1016/j.polymdegradstab.2018.06.001
- Yeo, J. C. C., J. K. Muiruri, W. Thitsartam, and Z. Li. 2018. "Recent Advances in the Development of Biodegradable PHB-Based Toughening Materials: Approaches, Advantages and Applications." *Materials Science and Engineering: C* 92: 1092–1116. doi:10.1016/j.msec.2017.11.006
- Zhang, X., L. Chen, T. Mulholland, and T. A. Osswald. 2019. "Effects of Raster Angle on the Mechanical Properties of PLA and Al/PLA Composite Part Produced by Fused Deposition Modeling." *Polymers for Advanced Technologies*. 30 (8): 2122–2135. doi:10.1002/pat.4645